Synthetic Jet Interaction With a Turbulent Boundary Layer Flow

Summary of Research

Principal Investigator:

DOUGLAS R. SMITH

Reporting Period:
April 11, 2001 – April 10, 2002

Department of Mechanical Engineering
University of Wyoming
1862 Land Grant Institution
P. O. Box 3295
Laramie, WY 82071-3295

Grant Number:
NAG-1-01063

1 Introduction

Perhaps one of the more notable advances to have occurred in flow control technology in the last fifteen years is the application of surface-issuing jets for separation control on aerodynamic surfaces. The concept was introduced by Johnston and Nishi (1990) who proposed using circular jets, skewed and inclined to the wall, to generate streamwise vortices for the purpose of mitigating boundary layer separation. The skew and inclination angles have subsequently been shown to affect the strength and sign of the ensuing vortices. With a non-circular orifice, in addition to skew and inclination, the yaw angle of the major axis of the orifice can influence the flow control effectiveness of the jet. In particular, a study by Zhang and Collins (1997) revealed that a non-circular orifice, yawed relative to the freestream, can be used to control the size and strength of the vortices produced by the control jet.

This early work used jets with only a steady injection of mass. Seifert et al. (1993) revealed that an unsteady blowing jet could be as effective at separation control as a steady jet but with less mass flow. Seifert et al. showed that small amplitude blowing oscillations superimposed on a low momentum steady jet was the most effective approach to delaying separation on a NACA 0015 airfoil at post-stall angles of attack.

More recent work suggests that perhaps the most efficient jet control effect comes from a synthetic (oscillatory) jet where the time-averaged mass flux through the orifice is zero, but the net wall normal momentum is non-zero. The control effectiveness of synthetic jets has been demonstrated for several internal and external flow fields (Amitay et al. 1998; Smith et al. 1998; Amitay et al. 2000). Smith et al. (1998) used synthetic jet control on a thick, blunt-nosed airfoil to delay stall well beyond the stall angles for the uncontrolled airfoil and with a dramatic increase in the lift-to-drag performance. Amitay et al. (2000) used an array of synthetic jets to mitigate flow separation in curved and diffusing ducts.

While the control effectiveness of synthetic jet actuators in an application setting has been confirmed through a number of studies, the fluid dynamic mechanism by which control is effected is not well understood. Issues like yaw angle and velocity ratio that have been studied for steady control jets have not been investigated for synthetic jets. Moreover, the role played by the inherently unsteady nature of a synthetic jet in the interaction with the controlled flow is not known. Some recent work by Rinehart and Glezer (1999) and Smith (2002) suggests that away from the immediate vicinity of the jet orifice the flow field is steady in the mean, and that the interaction of a synthetic jet and a boundary layer creates a secondary flow in the boundary layer consisting primarily of streamwise vortices.

To evaluate the efficiency of a synthetic jet at reducing the boundary layer susceptibility to separation, we must evaluate the role of actuator configuration and design on the control effect. For example, to mix high-momentum fluid from the edge of the boundary layer with low-momentum fluid near the wall, a streamwise vortex structure must be of the same size as the boundary layer thickness. The streamwise vortices originating from the interaction between a synthetic jet actuator and a cross-flow boundary layer would be expected to have a size that is initially determined by the penetration depth of the jet. For a rectangular steady jet, Weston and Thames (1979) have shown that the penetration depth will depend on the orientation, or yaw, of the major axis of the orifice relative to the mean cross-stream velocity direction. Perhaps of equal importance in determining the penetration depth and ensuing flow structure is the velocity ratio (jet-to-freestream) and duty cycle. For steady jets issuing into a cross-flow, the penetration depth has been shown to scale directly with the velocity ratio (Broadwell and

Breidenthal 1984). If the jet is pulsed, there exists a range of frequencies where the penetration is also frequency dependent and duty cycle dependent (Eroglu and Breidenthal 1991; Chang and Vakili 1995). Pulsed jets at low frequencies with short injection times (and short duty cycles) penetrate deeper into the cross-flow (Johari et al. 1999).

To improve the design and implementation of synthetic jet actuators in flows requiring active control, a better understanding of the character and structure of the interaction between the jet and the embedding boundary layer is required. To explore in greater detail the issues governing the nature of this interaction, we proposed to investigate the role of three parameters in the interaction of a synthetic jet with a turbulent boundary layer flow. These parameters were the yaw angle of the orifice relative to the incoming boundary layer flow, the ratio of synthetic jet velocity to the cross-flow velocity and the duty cycle of the actuator driver signal.

2 Project Goals

In this study, we sought to identify the role of orifice orientation (yaw angle) on synthetic jet flow control effectiveness, to estimate a range of yaw angles for optimum control, and to evaluate the role of velocity ratio and duty cycle on the penetration depth and the physical scale of the interaction. In the far-field of the synthetic jet boundary layer interaction where the flow is steady, the velocity profile shape and mean turbulence statistics were used in the evaluation. In the near-field where the flow is periodic, we used phase-locked measurements to build a dataset of velocity measurements with high spatial resolution in the yz plane. The intent was to use this dataset to develop a conceptual model of the flow-field. Using this conceptual model, we expected to confirm that streamwise vortices are the dominant feature of this interaction, to discover how these vortices are formed, and to understand which factors (i.e. yaw angle, velocity ratio and duty cycle) in the implementation of synthetic jet actuators affect their behavior.

3 Experimental Approach

The experiments were performed in the low-speed wind tunnel at the University of Wyoming Aerodynamics Laboratory. The boundary layer flow developed on a flat plate mounted parallel to the test section floor. The leading edge of the plate was a 4:1 ellipse, and transition occurred naturally near the leading edge of the plate. The plate was adjusted to have a zero pressure gradient along the length and uniform pressure across the width. Measurements of the surface pressure coefficient (C_p) varied by less than 1% along the length of the plate.

The synthetic jet actuator was driven using two 50 mm piezoelectric disks mounted on opposite sides of the actuator cavity. The orifice of the actuator was rectangular with dimensions, 50 mm (L) by 0.51 mm (h). The actuator was mounted in a circular plug, and the plug was installed flush with the surface of the flat plate. A retaining ring secured the plug in the plate and allowed the plug to be rotated continuously through 360° (figure 1). The yaw angle of the orifice, β, corresponded to the angle the major axis of the orifice made with the freestream direction, i.e. for $\beta = 0°$ the orifice axis and freestream velocity vector were parallel. Positive values of β were measured counter-clockwise (CCW) when the actuator is viewed from above. Three values of β were investigated: 0°, 10° and 20°.

All boundary layer measurements were obtained with a nominal freestream velocity of 17.0 $\pm$ 0.5 m/s. For all test cases, the boundary layer upstream of the actuator was turbulent. The

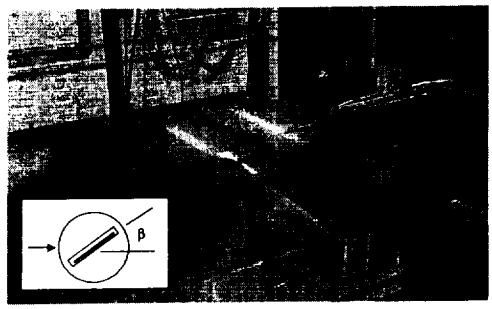

Figure 1: Photograph of the synthetic jet actuator and mounting plug in the test surface.

boundary layer thickness (δ_o) at a position immediately upstream of the actuator plug was 9.7 mm. A reference coordinate system was located at the center of the actuator orifice with x in the streamwise direction, z in the cross-span direction and y measured normal to the wall. Since the edge of the boundary layer may be obscured by the synthetic jet, all figures presented below show the distance from the wall (y) scaled by the upstream boundary layer thickness (δ_o). The cross-span distance (z) is normalized using the actuator orifice width, h.

Mean and fluctuating velocity measurements were acquired using a single normal-sensor hot-wire. The hot-wire was operated in constant temperature mode using an AA Labs AN-1003 constant temperature anemometer. The hot-wire probes were miniature-sensor boundary layer probes manufactured by Auspex Corporation. The wire was 5 μm in diameter with a 1.2 mm active length. Static hot-wire calibrations were performed *in situ* using a King's Law fit. The freestream flow temperature was recorded both during the calibration and during the boundary layer surveys. To account for flow temperature drift during a survey, all hot-wire voltages were corrected to a reference temperature.

The mean and fluctuating hot-wire signals were measured independently after low-pass (10Hz) and bandpass (10Hz - 4KHz) filtering, respectively. A Stanford Research Systems model SR640 was used to filter the signals. All probe motion control and data acquisition were performed using National Instruments cards and Labview software. At each point in a boundary layer survey, 96K data points were obtained at a sampling rate of 10KHz. In the data acquisition, the actuator driver signal was also recorded to permit phase-locked analysis of the hot-wire signal.

The synthetic jet actuator performance was tested in a quiescent environment prior to installation in the wind tunnel test. The actuator was calibrated by recording the velocity signal, $u(t)$, from a hot-wire placed in the plane of the orifice, along the orifice centerline. The outstroke portion of this velocity trace was identified and used to estimate a velocity U_o defined as L/τ where L is the effective stroke length of the actuator, ($L = \int_0^\tau u(t)\,dt$) and τ is one-half the period of the actuator forcing signal (see Smith and Glezer 1998). Assuming a sinusoidal variation in velocity at the orifice, U_o is equal to $2U_{max}/\pi$ where U_{max} is the peak velocity measured by the hot-wire during the outstroke of the actuator. In these experiments, U_o was estimated to be 14 m/s. The optimum operational frequency of the actuator (f = 500 Hz), where the orifice velocity reached a maximum, was found by varying the driving frequency in 10 Hz steps and recording the peak velocity at the orifice.

To permit comparisons with studies involving a steady jet in a cross-flow, a velocity ratio, R, can be defined as the ratio of the representative actuator velocity, U_o, to the freestream

velocity, U_∞. In the current set of experiments, we estimated R to be 0.82.

4 Project Accomplishments

Using the techniques described above, this study was to explore the influence of yaw angle, velocity ratio and duty cycle on the flow control effectiveness of a synthetic jet embedded in a cross-flow boundary layer. Initially, four yaw angles (0°, 30°, 60°, 90°) and three velocity ratios (0.5, 1.0, 2.0) were to be tested. The first estimates of the actuator velocity gave a velocity ratio of 1.0 with a freestream cross-flow velocity of 17 m/s. However, a calibration after the boundary layer surveys were completed revealed a lower velocity at the orifice, and subsequently, the velocity ratio for these tests was revised downward to 0.82. The early focus of the experiments was on identifying the effect of yaw angle on the interaction, and preliminary tests revealed that with the current velocity ratio (R = 0.82) and a yaw angle greater than 20°, a very weak interaction, confined to a narrow region near the wall, was apparent. Consequently, we considered a revised set of yaw angles: 0°, 10°, 20°.

For each yaw angle, β, profiles of the instantaneous velocity in the boundary layer were measured at two positions downstream of the actuator ($x/L = 1.0, 1.45$). At each streamwise position, the boundary layer profiles were obtained at multiple cross-span positions. These profiles were separated in the cross-span direction by $3.125h$ and extended from the wind tunnel centerline to the edge of the jet boundary layer interaction on either side. Time- and phase-averaging were performed on the instantaneous velocity signals to obtain averaged boundary layer profiles.

Note that a single, normal hot-wire is insensitive to flow direction. In this experiment, velocities normal to the wall would tend to increase the apparent streamwise velocity, and cross-span velocities would have the opposite effect. Measurements by Zhang and Collins (1997) with LDA in the boundary layer downstream of steady rectangular jet with velocity ratio of 1.0 showed velocities in the y-z plane that were at most 10% of the mean freestream velocity. This suggests that while there certainly is some corruption of the velocity measurements by wall-normal and cross-span velocities, the hot-wire is measuring predominantly streamwise velocities.

4.1 Time-averaged Measurements

The time-averaged velocity profiles are presented in order of $\beta = 0°, 10°$ and 20°, respectively. For $\beta = 0°$, the flow-field exhibited symmetry with respect to the centerline of the actuator, and consequently only measurements for $z/h \geq 0$ will be presented.

4.1.1 $\beta = 0°$

Figure 2 shows the cross-span change in the mean velocity profiles at the two streamwise locations $x/L = 1.0, 1.45$. The measured upstream profile (shown as a solid line) is included for reference. At $x/L = 1.0$ (figure 2(a)), the velocity profiles are characterized by severe distortion extending from $y/\delta_\circ = 0.2$ (along the centerline) to beyond the edge of the boundary layer. The shape of this distortion is reminiscent of a wake and in subsequent text will referred to as the velocity defect region. The vertical extent of the defect decreases away from the centerline of the interaction, and the height in the boundary layer at which the defect starts increases with z/h. The top of the velocity defect (near $y/\delta_\circ = 1.4$) shifts slightly towards the wall for profiles away

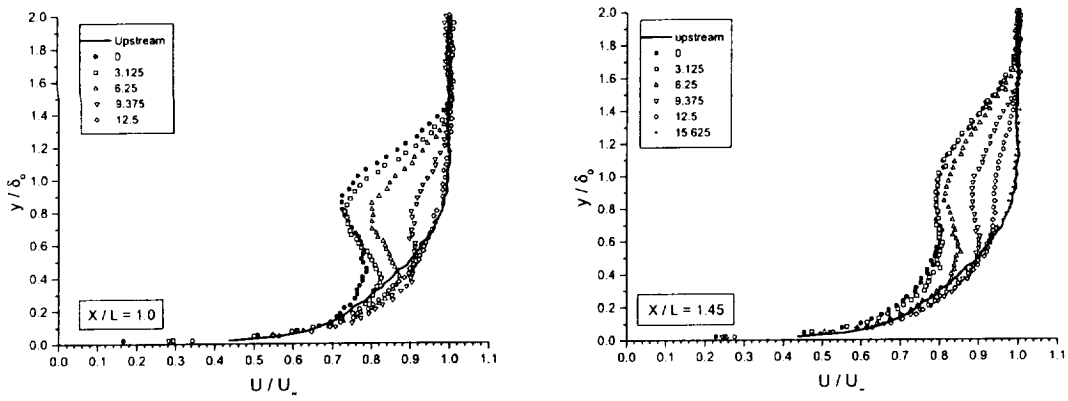

(a) x / L = 1.0

(b) x / L = 1.45

Figure 2: A cross-span comparison of the mean streamwise velocity profiles for $\beta = 0^o$.

from the centerline, but not to the same extent that the bottom of the defect moves away from the wall. This suggests that the defect region has an elliptical cross-section. In the centerline profile, the minimum in the defect occurs at a height of $y/\delta_o = 0.88$. For off-center profiles, the minimum shifts down in the boundary layer to $y/\delta_o = 0.8$ and is roughly constant with increasing z/h. For the outboard profiles (see profile at $z/h = 9.375$ and $y/\delta_o < 0.5$, figure 2a), a slight overshoot in the velocity profile (relative to the upstream profile) is apparent beneath the defect region and may be due to a weak counter-rotating vortex pair structure present in the defect region.

At $x/L = 1.45$ (figure 2b), the defect region has grown into the freestream, towards the wall and in the cross-span direction. The flow is becoming more uniform near the centerline of the interaction. The velocity minimum in the defect is decreasing presumably as turbulence mixes higher momentum fluid from the surroundings into this region. The fuller velocity profile below the defect region is less apparent at this streamwise position than in the upstream profiles.

An estimate of the spanwise scale for the interaction can be obtained from a consideration of how the cross-span profiles change with increasing distance from the centerline. The vertical scale may be partially understood by noting that the orifice length L is approximately five times larger than the incoming boundary layer thickness, δ_o. Also note that δ_o/h is approximately 19. If, during the formation phase, the jet has a width of $5h$ (see Smith and Glezer(Smith and Glezer 1998)), then as the jet interacts with the boundary layer its width increases by a factor of five. As a percentage of the incoming boundary layer thickness (δ_o), the interaction attains a width of approximately one boundary layer thickness within one orifice length of its inception. Continuing downstream, the interaction continues to grow in the y and z directions. However, from the mean velocity profiles, it appears that the top of the interaction is becoming flatter. At both $x/L = 1.0$ and 1.45, the vertical and spanwise lengths of the interaction are equal, $1.2\delta_o$ and $1.6\delta_o$, respectively.

The mean velocity profiles at $x/L = 1.0$ suggest that a weak counter-rotating vortex pair may be present in the boundary layer. The rotation of this vortex pair would tend to draw low

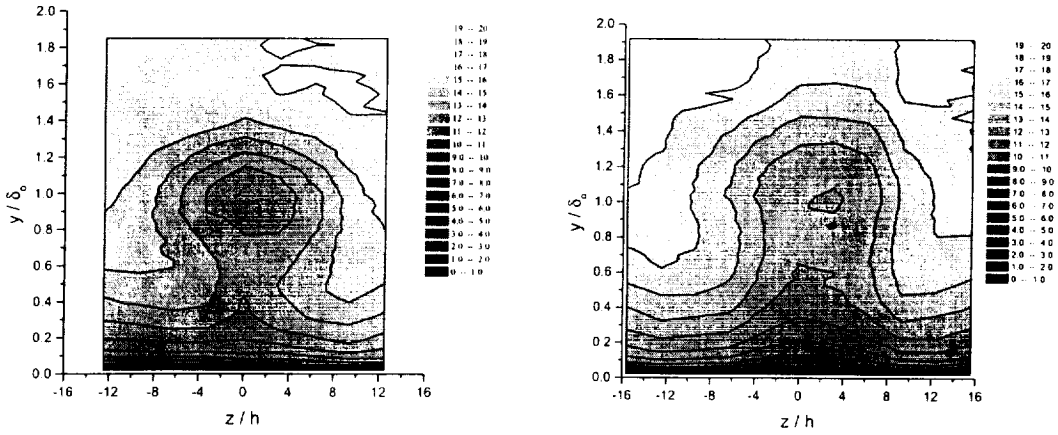

(a) x / L = 1.0 (b) x / L = 1.45

Figure 3: Contours of the mean streamwise velocity for $\beta = 0^o$.

momentum fluid up along the centerline of the interaction and push high momentum fluid down in the boundary layer along the sides of the interaction. Figure 3(a) shows a gray-scale contour map of streamwise velocity constructed from the individual cross-span profiles at $x/L = 1.0$. This figure shows that low momentum fluid has been drawn up along the centerline and that high momentum fluid is being pushed down in the boundary layer off-center. The effects are subtle indicating the vortex pair is likely weak, but persistent, as the same velocity trends are observed at $x/L = 1.45$ (figure 3b).

Figure 4 shows the cross-span variation in the streamwise turbulence intensity, u'_{rms}/U, at $x/L = 1.0, 1.45$. For all z/h positions at $x/L = 1.0$ (figure 4a), the peak intensity occurs at a position higher in the boundary layer than the position of the minimum in the mean velocity defect. Moreover, while the mean velocity defect remained at approximately the same elevation in the boundary layer with increasing z/h, the peak intensity moves progressively towards the wall with increasing z/h. At $y/\delta_o = 1.5$, there is still a non-negligible turbulence intensity despite the mean velocity profiles suggesting that this is the edge of the jet. This effect is perhaps due to an oscillation in the local freestream at the actuator driver frequency and will be examined in greater detail in the phase-averaged measurements. Finally, while the mean velocity profile at $z/h = 12.5$ appears uninfluenced by the jet interaction, the turbulence intensity profile shows an elevated fluctuation level in the boundary layer above $y/\delta_o = 0.5$.

At $x/L = 1.45$ (figure 4b), the peak turbulence intensity has dropped to a level of approximately 12.5% while broadening and moving away from the wall. The peaks in the off-center profiles have moved away from the wall more rapidly than the peak in the centerline profile. Also, this movement appears to be more pronounced than the movement in the mean velocity defect.

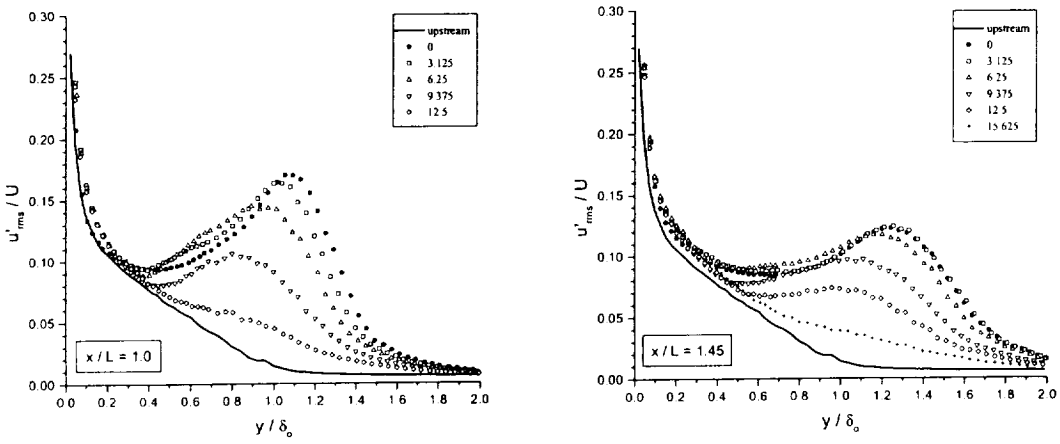

(a) x / L = 1.0

(b) x / L = 1.45

Figure 4: A cross-span comparison of the streamwise turbulence intensity profiles for $\beta = 0°$: x / L = 1.0, 1.45.

4.1.2 $\beta = 10°$

For $\beta = 10°$, the actuator is no longer symmetrically oriented about the x-y plane. In rotating the orifice through 10°, the cross-span length of the jet, as seen by the incoming flow, increased to approximately 8.7 mm from a value of 0.5 mm when $\beta = 0°$. The leading edge of the orifice was displaced to $z/h = +8.7$, and the trailing edge was displaced into $z/h = -8.7$. In this case, velocity profiles for $\pm z/h$ positions are shown.

Figure 5 shows the cross-span variation in the mean velocity profiles at $x/L = 1.0$. The first point to note in these profiles is that, in comparison with $\beta = 0°$, the height to which the interaction rises in the boundary layer is considerably reduced, confined now to the lower 60% of the boundary layer. This effect is clearly due to the broader initial cross-section of the jet. The centerline profile exhibits a small region of constant velocity between $y/\delta_o = 0.1$ and $y/\delta_o = 0.3$. For $z/h > 0$ (figure 5a), the mean velocity near the wall initially decreases before filling in farther off center. In shape, all of the profiles here appear to be less full than the upstream mean velocity profile, and because the jet does not penetrate as deeply into the boundary layer, the defect region appears closer to the wall. For $z/h < 0$ (figure 5b), the mean velocity profiles change monotonically as distance from the centerline increases, with the defect region becoming shallower. Note that while the velocity defect does fill in, the profiles out to $z/h = -15.625$ all exhibit an inflection point, and near the wall, there is a small region in the profiles between $z/h = -6.25$ and -12.5 where the velocity appears to overshoot the upstream profile. This is likely due to fluid that is swept in along the wall in the lee of the jet. A low pressure region in the lee of the jet would tend to draw fluid into this region from the sides of the jet. Since the trailing edge of the orifice (located at $z/h = -8.7$) is closer to the measurement plane, the overshoot in the mean velocity profiles near the wall for $z/h < 0$ may be a consequence of the fluid accelerating into the low pressure region.

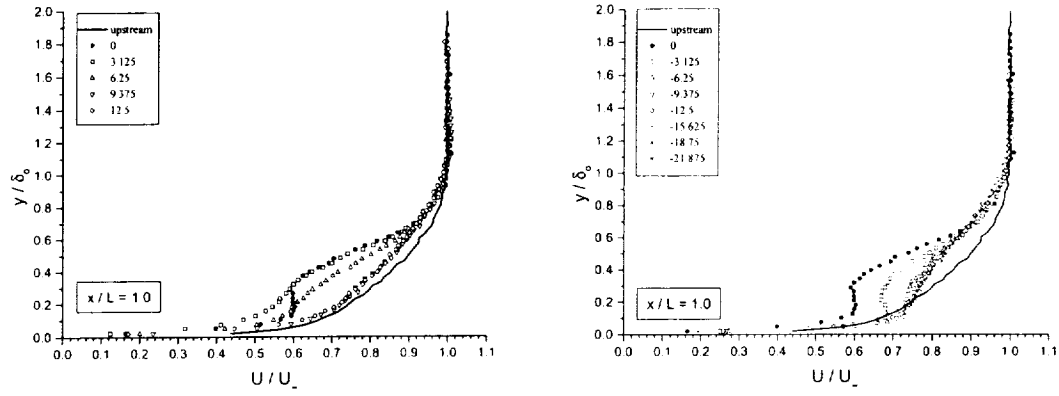

(a) (b)

Figure 5: A cross-span comparison of the mean streamwise velocity profiles for $\beta = 10^o$: x / L = 1.0.

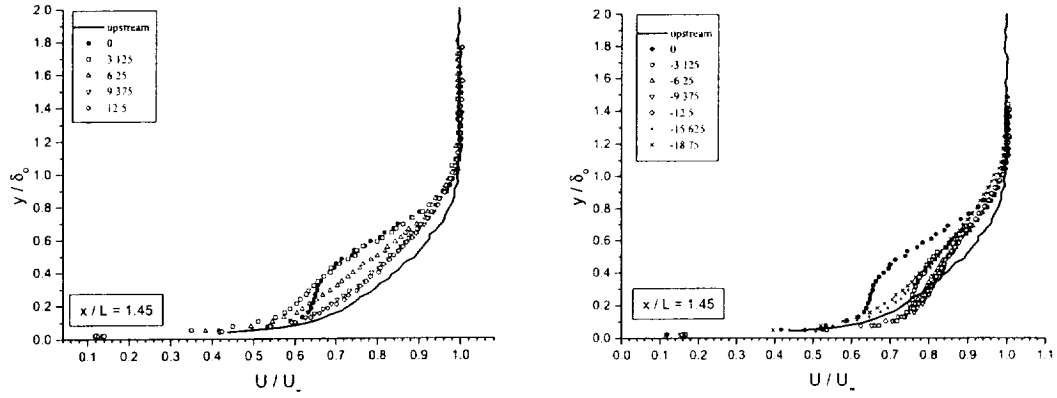

(a) (b)

Figure 6: A cross-span comparison of the mean streamwise velocity profiles for $\beta = 10^o$: x / L = 1.45.

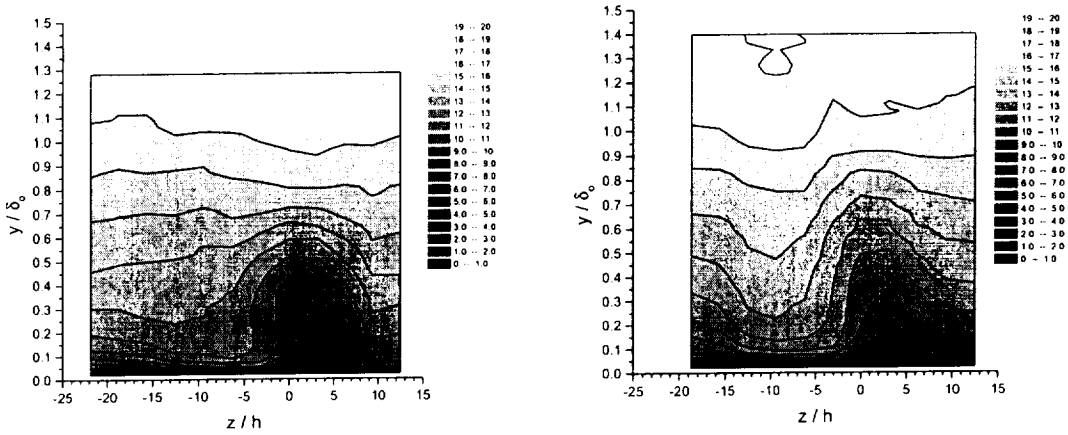

(a) x / L = 1.0 (b) x / L = 1.45

Figure 7: Contours of the mean streamwise velocity for $\beta = 10^o$.

At $x/L = 1.45$, the profiles for $z/h \geq 0$ (figure 6a) appear qualitatively similar to the profiles at $x/L = 1.0$. The defect region in the profile has grown only slightly in height while not appearing to have grown at all in the cross-span direction. For $z/h < 0$ (figure 6b), there appears to be a non-monotonic change in the velocity profiles with the profile at $z/h = -15.625$ exhibiting a region of constant mean velocity gradient above $y/\delta_\circ = 0.2$. The velocity overshoot observed near the wall at $x/L = 1.0$ now includes the profile at $z/h = -3.125$, but disappears from the profiles very rapidly between $z/h = -12.5$ and $z/h = -15.625$.

Figure 7 shows gray-scale contour maps of the streamwise velocity constructed from the individual cross-span profiles. In these figures, the mean velocity distribution is consistent with a single vortex structure showing high momentum fluid near the wall for $z/h < 0$, and low momentum away from the wall for $z/h > 0$. At $x/L = 1.0$ (figure 7a), the effect of the vortex is mostly felt in the lower half of the boundary layer. However, at $x/L = 1.45$ (figure 7b), the scale of the distortion reaches the edge of the boundary layer and extends over $25h$ in the cross-span direction.

To assist with the interpretation of the mean velocity contour maps, a comparison was made with the measurements of Zhang and Collins (1997), who studied the interaction of a boundary layer with a steady rectangular jet. In that study, the velocity measurements showed very clearly the existence of a single streamwise vortex in the lee of the jet. By comparison, the mean velocity contours here (figure 7) suggest the presence of a single vortex with a counter-clockwise sense of rotation (looking downstream at the vortex). A vortex of this sense would lead to a down-draft of high momentum fluid for $z/h < 0$ and an up-draft of low momentum fluid for $z/h > 0$.

Figure 8 shows the cross-span variation in the streamwise turbulence intensity at $x/L = 1.0$. As seen in the measurements for $\beta = 0°$, the peak in the turbulence intensity profile occurs higher in the boundary layer than the minimum defect in the mean velocity profiles. This may be due to the higher mean shear at this height in the boundary layer. For $z/h > 0$, the

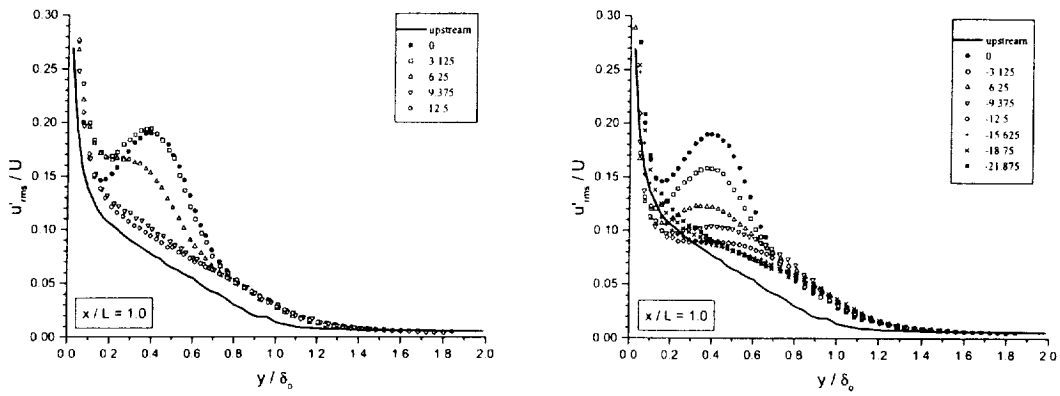

(a) (b)

Figure 8: A cross-span comparison of the streamwise turbulence intensity profiles for $\beta = 10^o$: x / L = 1.0.

peak in the turbulence intensity profiles falls off quickly with z/h, showing little change for $z/h > 9.375$. For $z/h < 0$, the peak in the profiles changes more slowly, with the peaks at $z/h = -9.375, -12.5$ appearing to shift away from the wall. In the region $0.1 < y/\delta_o < 0.3$, the turbulence intensity profiles have fallen below the upstream profile, a consequence of the higher mean velocity in this region.

At $x/L = 1.45$ (figure 9), the peaks in the turbulence intensity profiles have decreased and become broader. The trends in the profiles for $z/h > 0$ are similar to those observed at $x/L = 1.0$. For $z/h < 0$, the region of suppressed turbulence intensity now extends to $y/\delta_o = 0.4$. Unlike the profile shapes in the outer part of the boundary layer for $z/h > 0$, the $z/h < 0$ profile shapes all exhibit a slight increase over the upstream intensity levels for $y/\delta_o > 0.5$. These profile shapes and the mean velocity profiles are consistent with low momentum fluid, with high turbulence levels, having been swept away from the wall.

4.1.3 $\beta = 20°$

For $\beta = 20°$, the projected area of the jet was approximately 17 mm, with the leading edge of the orifice at $z/h = +17$ and the trailing edge at $z/h = -17$.

Figure 10 shows the cross-span variation in the mean velocity profiles for $x/L = 1.0$. The presence of the synthetic jet in the boundary layer is much less pronounced in these profiles and is confined to the lower 50% of the boundary layer. The largest velocity defects appear in the profiles between $z/h = 6.25$ and 12.5 (figure 10a) with the centerline profile showing the smallest deviation from the upstream profile. For $z/h < 0$ (figure 10b), the profiles are all fuller than the profiles on the other side of the centerline, a consequence perhaps of a weak longitudinal vortex drawing high momentum fluid from the outer region of the boundary layer to the wall.

At $x/L = 1.46$ (figure 11), the mean velocity profiles for $z/h > 0$ become more similar in

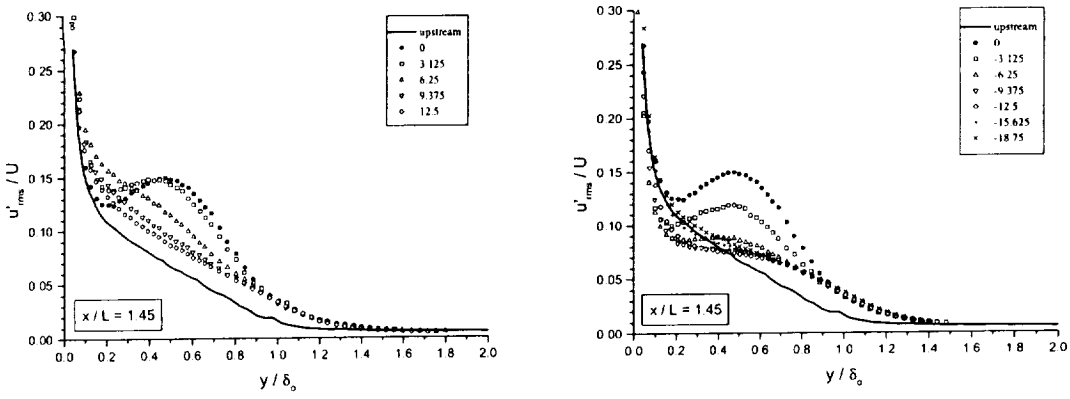

(a) (b)

Figure 9: A cross-span comparison of the streamwise turbulence intensity profiles for $\beta = 10°$: x / L = 1.45.

shape, and a constant mean velocity gradient appears throughout most of the boundary layer for $z/h \geq 9.375$. For $z/h < 0$, the mean velocity profiles have become fuller near $y/\delta_o = 0.2$, but farther from the wall are mostly unchanged from $x/L = 1.0$.

Gray-scale contour maps of the mean streamwise velocity are shown in figure 12. In this case, the mean flow structure is consistent with that observed for $\beta = 10°$, and a single vortex may be present near $z/h = 5$. The size and strength of the vortex appears to be quite a bit reduced over the $\beta = 10°$ case, but the distortion to the boundary layer is evident nevertheless.

The turbulence intensity profiles for $x/L = 1.0$ are shown in figure 13. These profiles reveal that the synthetic jet has a greater effect on the boundary layer than the mean velocity profiles would suggest. In figure 13(a) ($z/h \geq 0$), the centerline profile exhibits the lowest turbulence intensity on this side of the interaction. As z/h increases, the turbulence intensity profile increases monotonically to $z/h = 15.625$ before dropping off abruptly and changing shape at $z/h = 18.75$. Note that the projection of the orifice into the yz-plane lies between $\pm 17 z/h$. The abrupt change in the turbulence intensity profile near $+17 z/h$ suggests that the synthetic jet interaction is confined to the region immediately downstream of the orifice. Also of interest in figure 13(a) is that, of the three values of β considered, the highest peak in the turbulence intensity profiles occurred at $\beta = 20°$ and $z/h = 15.625$. Of course, the defect region is also closest to the wall of the three angles, and relatively, the turbulence would be the highest in this region. For $z/h < 0$ (figure 13b), there is small undulation in the profiles with z/h, first decreasing away from the centerline then increasing before finally decreasing at the edge of the interaction. Overall, the turbulence intensity is much more subdued than for $z/h > 0$.

At $x/L = 1.46$ (figure 14), the turbulence intensity profile at $z/h = 15.625$ is still the most amplified profile. As z/h decreases, the turbulence intensity profiles fall off monotonically to the actuator centerline. For $z/h \geq 0$ (figure 14a), the profiles all collapse to one curve, which shows at most a 50% increase in relative turbulence intensity over the upstream profile.

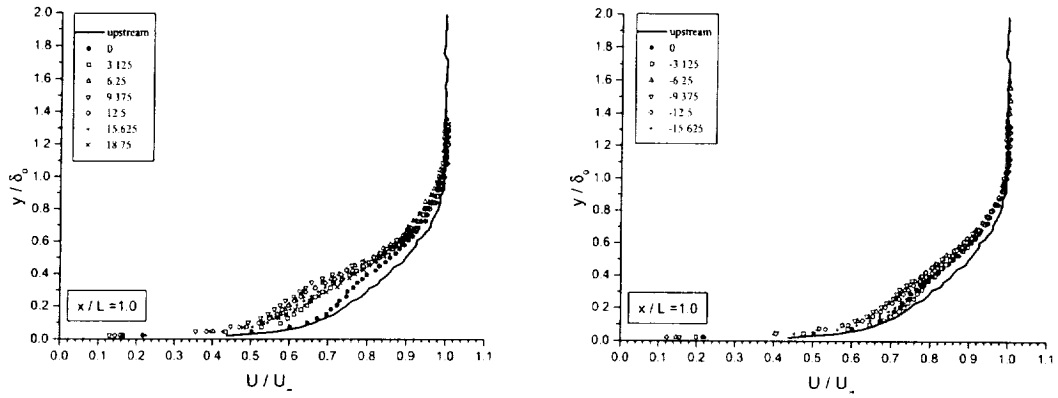

(a) (b)

Figure 10: A cross-span comparison of the mean streamwise velocity profiles for $\beta = 20^o$: x / L = 1.0.

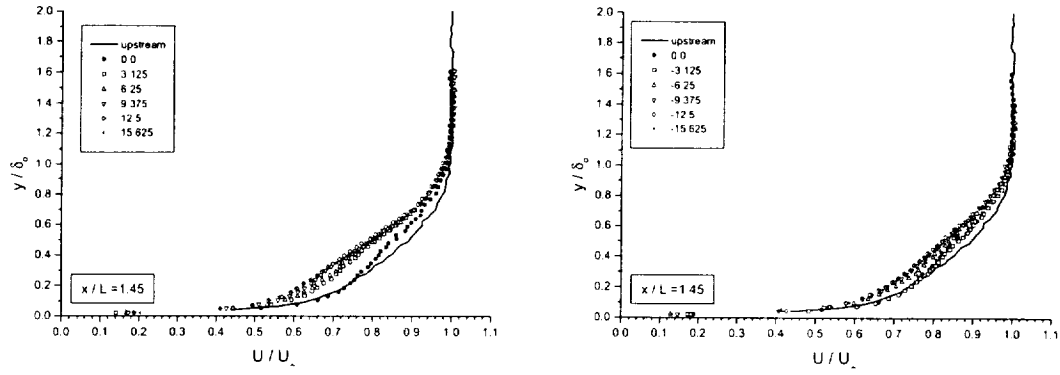

(a) (b)

Figure 11: A cross-span comparison of the mean streamwise velocity profiles for $\beta = 20^o$: x / L = 1.46.

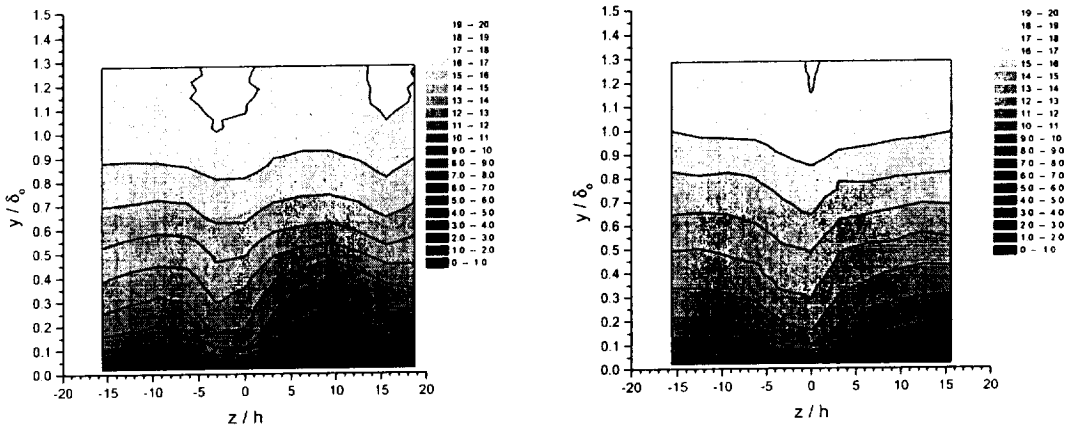

(a) x / L = 1.0 (b) x / L = 1.45

Figure 12: Contours of the mean streamwise velocity for $\beta = 20^o$.

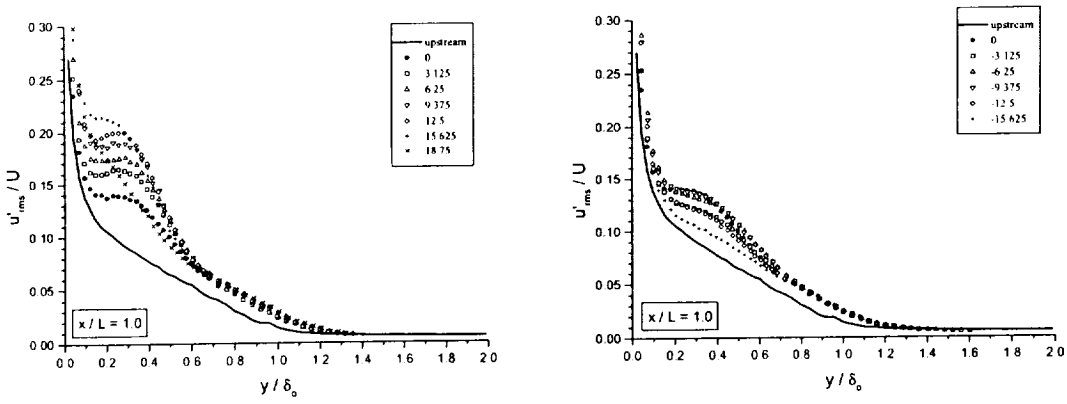

(a) (b)

Figure 13: A cross-span comparison of the streamwise turbulence intensity profiles for $\beta = 20^o$: x / L = 1.0.

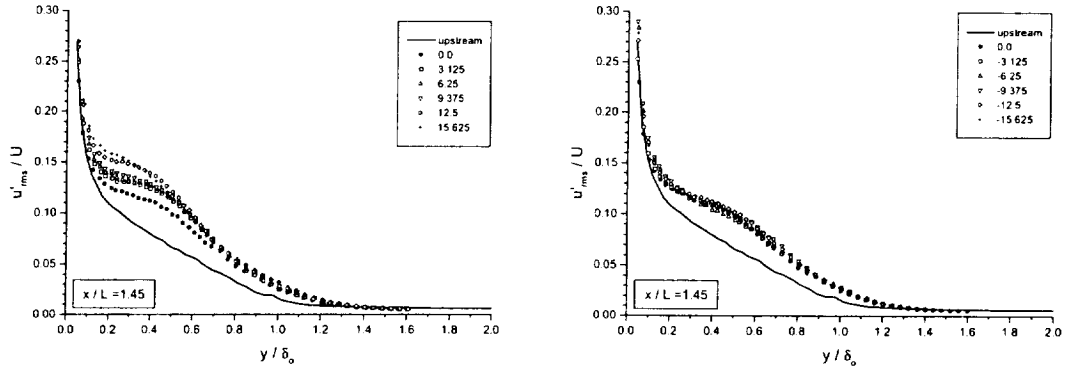

(a) (b)

Figure 14: A cross-span comparison of the streamwise turbulence intensity profiles for $\beta = 20^o$: x / L = 1.46.

4.2 Phase-averaged Velocity Profiles

By analyzing the hot-wire velocity signal and the actuator driver signal simultaneously, phase-averaged velocity profiles of the boundary layer were constructed. With a data sampling rate of 10KHz and an actuator driver frequency of 500Hz, twenty profiles, equally-spaced throughout the driver period, were obtained. For each point in a boundary layer profile, a linear interpolation scheme was used to shift the phase-averaged data to the same relative times in the actuator driver period. The angle, ϕ, is used to denote the phase in the period of the actuator driving signal.

4.2.1 $\beta = 0°$

Figure 15 shows the mean velocity profile at $z/h = 0$ for four phases of the actuator period $(0°, 90°, 180°, 270°)$. These figures show very clearly the "pulsing" of the defect region during one actuator cycle. From 0° to 180°, the mean velocity defect becomes shallower and shifts down in the boundary layer and is accompanied by a reduction in the vertical scale of the region. At 270°, the depth of the defect region has increased significantly with a steepening of the velocity gradients due to the smaller vertical scale of this region. In the last quarter of the period, the defect region rises rapidly from below $y/\delta_o = 0.8$ to above $y/\delta_o = 1.2$. Note that at the edge of the jet-boundary layer interaction there is an apparent phase-locked change in the local freestream velocity extending about $0.5\delta_o$ into the freestream.

Figure 16 shows phase-locked gray-scale contour maps of the streamwise velocity for the sequence of four phase angles shown above. Throughout the actuator cycle, the relative shapes of the contours are consistent with the structure proposed from an inspection of the time-averaged contours. This observation suggests that at this location the general features of the boundary layer structure are established but that the strength, scale and position are modulated at the actuator frequency. These figures show quite clearly the cross-stream (up and down) motion of the interaction during a single forcing cycle.

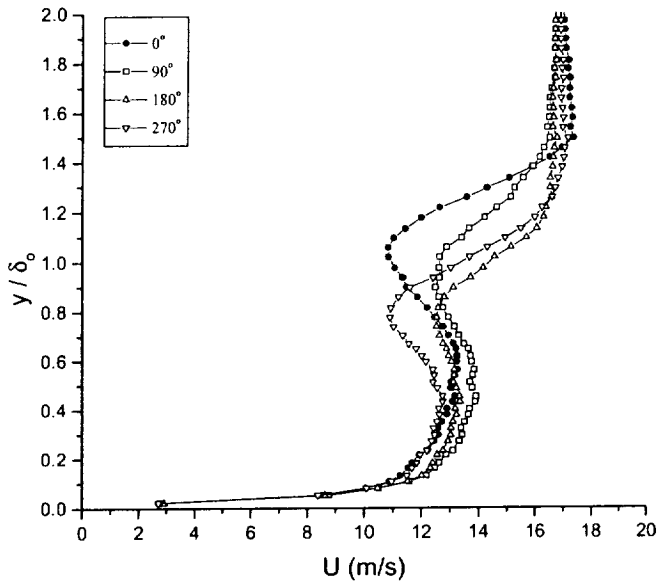

Figure 15: Phase-averaged mean streamwise velocity profiles for $\beta = 0^o$ at x / L = 1.0 and z / h = 0.0.

4.2.2 $\beta = 10°$

Figure 17 shows a sequence of gray-scale contour maps of streamwise velocity for $\beta = 10°$ at six phase angles ($\phi = 18°, 108°, 198°, 252°, 288°, 342°$). Unlike the phase-averaged profiles at $\beta = 0°$ where the flow structure remained coherent throughout the actuator cycle, these contours show that the flow-field changes quite significantly during the actuator cycle. For $z/h < 0$, the defect region appearing at $y/\delta_o = 0.3$, and signifying the core of the single vortex, collapses between $\phi = 198°$ and $288°$. This segment of the actuator cycle presumably corresponds to the suction phase when fluid in the boundary layer flows past the orifice mostly undeflected. During the blowing phase of the actuator cycle ($\phi = 18°$), the defect region is quite pronounced, and the jet contributes to the formation of a single longitudinal vortex. For $z/h < 0$, fluid with high streamwise momentum appears to be swept in towards the centerline from off-center, and the single vortex structure reappears.

5 Conclusions

The mean flow features in the boundary layer downstream of a wall-mounted synthetic jet were studied for three yaw orientations of the synthetic jet orifice. When the orifice was aligned with the mean freestream velocity ($\beta = 0°$), a flow structure consistent with a weak counter-rotating vortex pair was observed in the boundary layer. This structure was established within one orifice length downstream of the actuator center and appeared to be a steady feature of the flow but with an amplitude and position in the boundary layer that varied at the actuator driver frequency. For $\beta = 10°$, the mean velocity profiles across the span of the interaction suggested

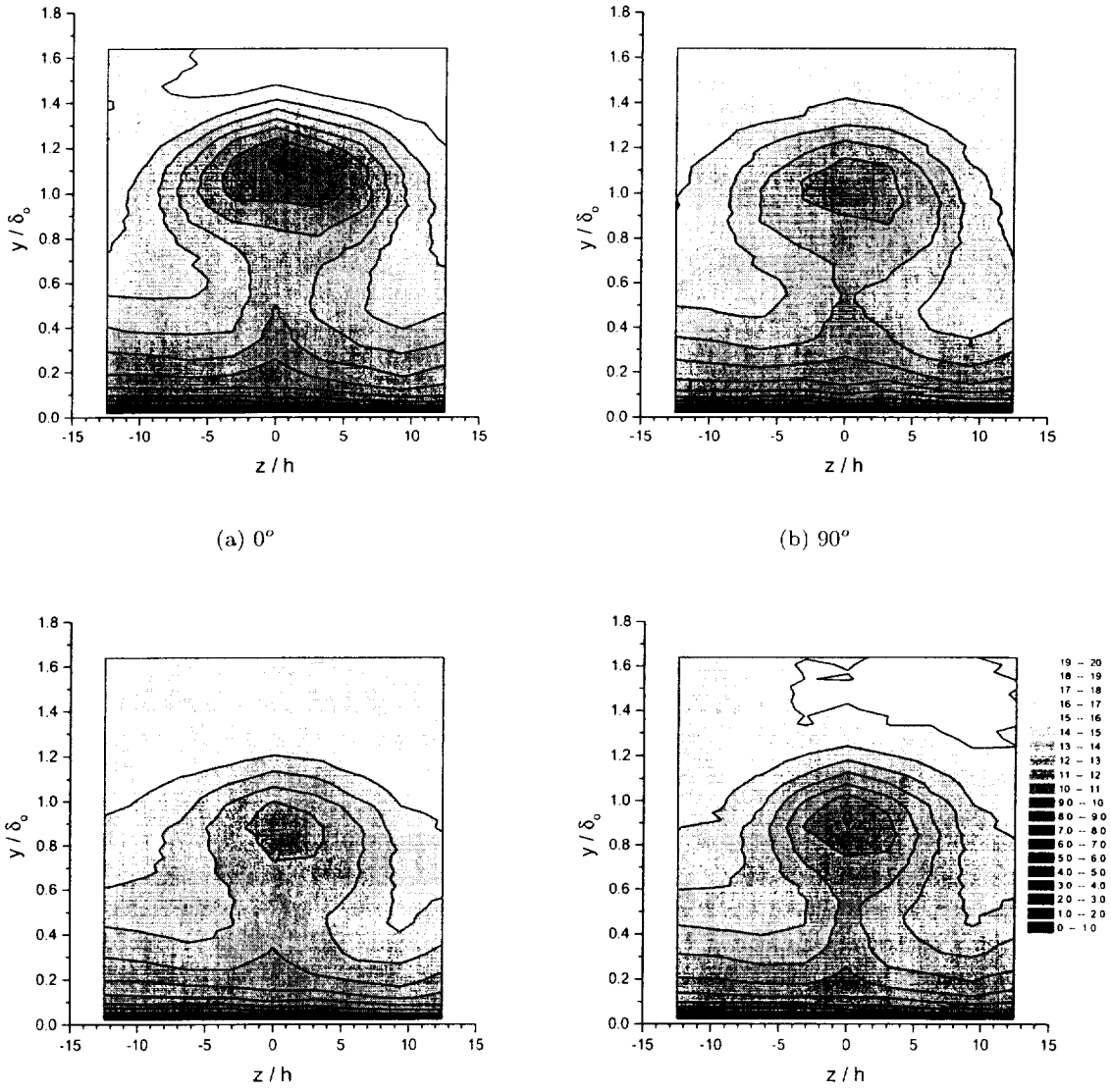

(a) 0^o (b) 90^o

(c) 180^o (d) 270^o

Figure 16: Phase-averaged contours of mean streamwise velocity for $\beta = 0^o$ at x / L = 1.0.

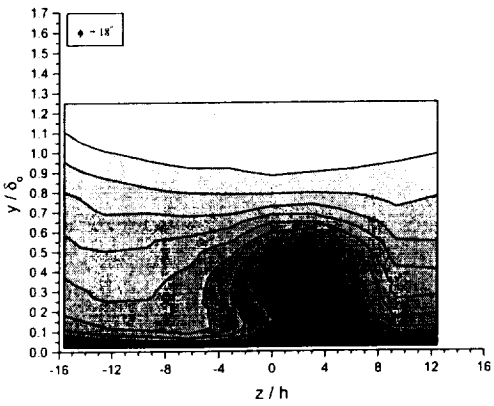

(a) 18^o

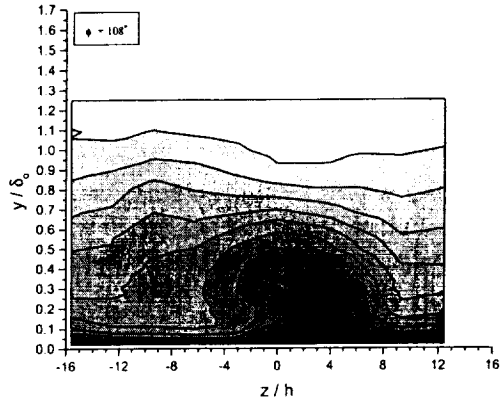

(b) 108^o

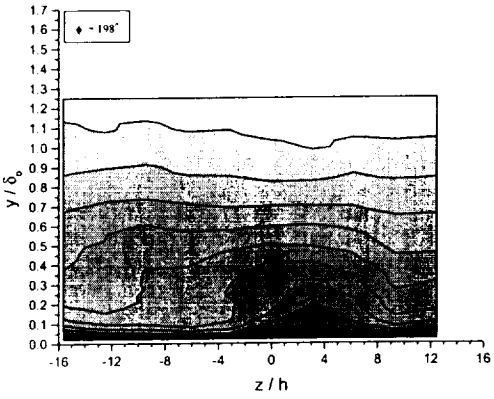

(c) 198^o

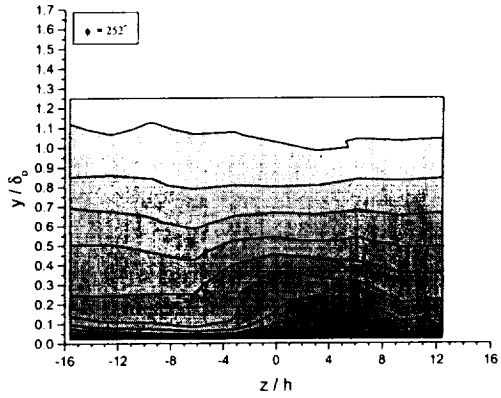

(d) 252^o

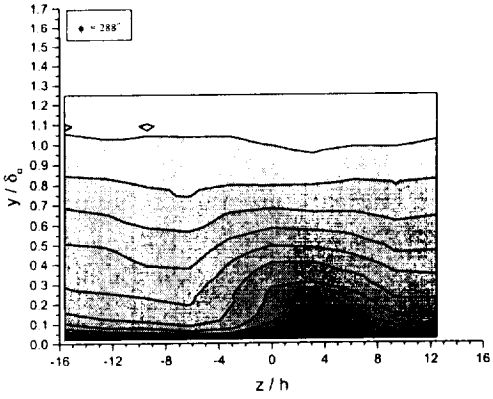

(e) 288^o

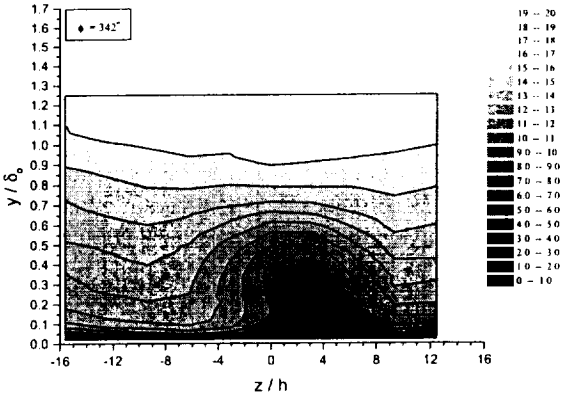

(f) 342^o

Figure 17: Phase-averaged contours of the mean streamwise velocity for $\beta = 10^o$ at x / L = 1.0.

the presence of a single vortex in the boundary layer. Looking downstream, the vortex had a counter-clockwise rotation, sweeping high momentum towards the wall for $z/h < 0$ and pushing low momentum up in the boundary layer for $z/h > 0$. For $\beta = 20°$, a similar structure appeared to be present, but weaker in strength than for the $\beta = 10°$ case. Also, phase-locked contours of the streamwise velocity in a yz plane at $x/L = 1.0$ for $\beta = 10°$ revealed a significant modulation of the single vortex structure during one actuator period.

For all β values, elevated streamwise turbulence intensity levels were observed in the boundary layer, but appeared to be due primarily to the synthetic jet and not to the redistribution of turbulence by any secondary flow structure present in the boundary layer.

6 Plans for future work

Due to the departure of the graduate student midway through the grant period, the set of measurements originally planned were not completed: only a single velocity ratio and duty cycle were studied. Once a new graduate student has been identified, our plan will be to complete the originally proposed measurements using phase-locked PIV to better resolve the three-dimensionality of the flow-field.

The measurements described above reveal that the interaction of a synthetic jet with a turbulent boundary layer creates a secondary flow downstream of the actuator with elevated turbulence levels near the wall. Both of these phenomena, the secondary flow and the elevated boundary layer turbulence, are known to increase the local heat transfer rate at the surface. To complement the velocity field measurements, the local surface heat transfer coefficient will be measured in the near-field of the actuator in an effort to understand how a synthetic jet actuator may be used to modify surface transport phenomena.

7 Publications

Bridges, A. B. and Smith, D. R., "The influence of orifice orientation on the interaction of a synthetic jet with a turbulent boundary layer," AIAA Paper 2001-2774, 31^{st} AIAA Fluid Dynamics Conference, Anaheim, CA, 2001.

8 Personnel

AMANDA BRIDGES, M.S. student. Ms. Bridges started her graduate program in September 2001, but dropped out in January 2002 for personal reasons.

DOUGLAS R. SMITH, Assistant Professor.

References

Amitay, M., D. Pitt, V. Kibens, D. Parekh, and A. Glezer (2000). Control of internal flow separtion using synthetic jet actuators. AIAA Paper 2000-0903, AIAA 38^{th} Aerospace Sciences Mtg., Reno, NV, January 10-13, 2000.

Amitay, M., B. L. Smith, and A. Glezer (1998). Aerodynamic flow control using synthetic jet technology. AIAA Paper 98-0208, AIAA 36th Aerospace Sciences Mtg., Reno, NV, January 12-15, 1998.

Broadwell, J. E. and R. E. Breidenthal (1984). Structure and mixing of a transverse jet in incompressible flow. *J. Fluid Mech. 148*, 405–412.

Chang, Y. K. and A. D. Vakili (1995). Dynamics of vortex rings in crossflow. *Phys. Fluids 7*(7), 1583–1597.

Eroglu, A. and R. E. Breidenthal (1991). Effects of periodic disturbances on structure and flame length of a jet in a cross flow. AIAA Paper 91-0137.

Johari, H., M. Pacheco-Tougas, and J. C. Hermanson (1999). Penetration and mixing of fully modulated turbulent jets in crossflow. *AIAA J. 37*(7), 842–850.

Johnston, J. P. and M. Nishi (1990). Vortex generator jets - means for flow separation control. *AIAA J. 28*(6), 989–994.

Rinehart, C. and A. Glezer (1999). Synthetic jet-based vortex generation for aerodynamic flow control. Paper AF7, 52nd APS - Division of Fluid Dynamics Meeting, New Orleans, LA.

Seifert, A., T. Bachar, D. Koss, M. Shepshelovich, and I. Wygnanski (1993). Oscillatory blowing: a tool to delay boundary-layer separation. *AIAA J. 31*(11), 2052–2060.

Smith, B. L. and A. Glezer (1998). The formation and evolution of synthetic jets. *Phys. Fluids 10*(9), 2281–2297.

Smith, D. (2002). The interaction of a synthetic jet with a cross-flow boundary layer. *AIAA Journal*. In press.

Smith, D. R., M. Amitay, V. Kibens, D. Parekh, and A. Glezer (1998). Modification of lifting body aerodynamics using synthetic jet actuators. AIAA Paper 98-0209, AIAA 36th Aerospace Sciences Mtg., Reno, NV, January 12-15, 1998.

Weston, R. P. and F. C. Thames (1979). Properties of aspect-ratio-4.0 rectangular jets in a subsonic crossflow. *J. Aircraft 16*(10), 701–707.

Zhang, X. and M. W. Collins (1997). Measurements of a longitudinal vortex generated by a rectangular jet in a turbulent boundary layer. *Phys. Fluids 9*(6), 1665–1673.